Soft Matter

PAPER

View Article Online
View Journal | View Issue

Cite this: *Soft Matter*, 2018, **14**, 9851

Hydrophobicity of surface-immobilised molecules influences architectures formed *via* interfacial self-assembly of nucleoside-based gelators†

Maria Galini Faidra Angelerou, [a] Bin Yang,[a] Thomas Arnold, [bcde] Jonathan Rawle,[b] Maria Marlow*[a] and Mischa Zelzer*[a]

Received 12th September 2018,
Accepted 7th October 2018

DOI: 10.1039/c8sm01868e

rsc.li/soft-matter-journal

Surface-mediated self-assembly has potential in biomaterial development but underlying rules governing surface–gelator interactions are poorly understood. Here, we correlate surface properties with structural characterization data of nucleoside-based gels obtained by GISAXS and GIWAXS and find that hydrophobicity descriptors (log *P*, polar surface area, aromaticity) are key predictors for the gel structures formed.

Introduction

Supramolecular gels have attracted significant interest as conducting materials, materials for energy and information storage, catalysis and sensors[1,2] and for biological applications in tissue engineering, drug delivery, cell culture and gene therapy.[1,3,4] A key requirement for the application of supramolecular gels is the fabrication of highly controlled nanoarchitectures that can perform predefined functions.

Surface-mediated self-assembly has recently emerged as a promising new approach to address this challenge as it aims to harness the universal presence of interfaces to influence the outcome of the self-assembly process.[5,6] Despite its promise, surface-mediated self-assembly has not yet demonstrated its full potential because our understanding of the underpinning relationship between surface properties and gel functionality is very limited. Surface properties such as hydrophilicity, roughness, charge and structure have been implicated in affecting self-assembly of small molecular weight gelators, leading to adaptation of different architectures,[7–9] geometries[10] or mechanical properties[11] of the self-assembled materials. However, currently data is unable to predict surface–supramolecular material property relationships.

To address this lack of mechanistic understanding and enable rational design of interfacial self-assembled structures, two challenges have to be met. Firstly, the structure of self-assembled architectures at interfaces rather than the bulk have to be measured. Here, we employ grazing angle incidence scattering on gel films for the first time to obtain insight in the self-assembled structures formed in a gel film. Secondly, correlations between surface parameters and supramolecular material properties have to be established. Here, we are correlating the structural data from the gel obtained by grazing incidence scattering with a range of experimental and theoretical descriptors of the surface to elucidate determinants that underpin the control imparted by surfaces on the self-assembled architectures (Fig. 1).

We hypothesize that the chemical similarity between the gelator and the surface chemistry leads to interference of the surface with the driving forces that underpin the self-assembly. Hydrophobic and solvophobic interactions have been reported

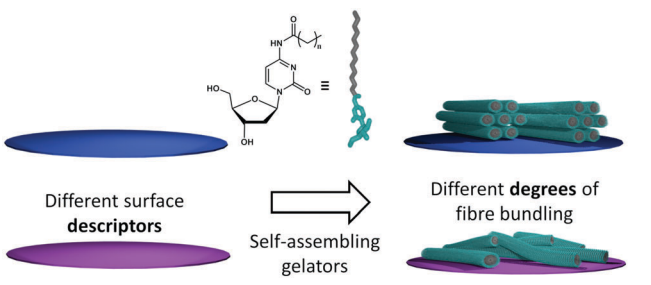

Fig. 1 Conceptual overview of the work investigating the correlations between different surface descriptors and the self-assembly of different 2′-deoxycytidine-based gelators (the 2′-deoxycytidine moiety is coloured green and the alkyl chain grey).

[a] *Department of Pharmacy, University of Nottingham, Nottingham, NG2 7RD, UK. E-mail: maria.marlow@nottingham.ac.uk, mischa.zelzer@nottingham.ac.uk*
[b] *Diamond Light Source Ltd, Harwell Science and Innovation Campus, Didcot, Oxfordshire, OX11 0DE, UK*
[c] *European Spallation Source ERIC, P.O. Box 176, SE-221 00 Lund, Sweden*
[d] *STFC, Rutherford Appleton Laboratory, Chilton Didcot, OX11 0QX, UK*
[e] *Department of Chemistry, University of Bath, Claverton Down, Bath BA2 7AY, UK*

† Electronic supplementary information (ESI) available: Experimental procedures, surface analysis, procedures for GIWAXS and GISAXS data processing, statistical analysis. See DOI: 10.1039/c8sm01868e

as key driving forces in self-assembly.[12–17] Previously, we have shown that an alkyl-modified derivative of cytidine produces gel films with different mechanical properties on a hydrophilic and a hydrophobic surface.[11] AFM measurements showed that the dried gels displayed fibres with larger diameters on the hydrophobic than on the hydrophilic surface.

Results and discussion

To test the hypothesis that hydrophobic surface interactions play a key role we first needed to establish if altering the chemical composition of the hydrophobic alkyl tail in the gelator is directly related to a change in fibre architecture, *i.e.* a change in fibre diameter. Four derivatives of a 2′-deoxycytidine-based gelator with varying alkyl chain lengths (C8-dCyt, C10-dCyt, C12-dCyt and C14-dCyt with 8, 10, 12 and 14 carbon atoms, respectively, Fig. S1, ESI†) were synthesised and used to prepare gel films on piranha cleaned silicon wafers (OH surfaces). This family of gelators was selected over other nucleolipid-based gelators under investigations[14,18–20] as they are synthesized through a straightforward, one-pot synthetic route,[21] their mechanism of self-assembly is well-understood[17] and they have shown promising potential in drug delivery applications.[21] The OH surfaces (surfaces covered with hydrophilic hydroxyl groups) were characterized with AFM (Fig. S2, ESI†) and water contact angle (WCA) measurements (Table S1, ESI†), showing that the surfaces are very hydrophilic (WCA = 4.7 ± 0.7°) and smooth (R_q = 1.031 ± 0.167 nm) with no topographical features.

All four gelators self-assemble into fibrous structures (Fig. S3, ESI†) and form gel films on the OH surfaces. To determine the structure of the gel, time resolved grazing incidence wide angle X-ray scattering (GIWAXS) data were collected (Fig. S4, ESI†). Grazing incidence X-ray scattering is well-established to determine film structures on surfaces;[22,23] here we capitalize on the suitability of our samples to undergo GI X-ray scattering analysis (low surface roughness) to study the interfacial structures of supramolecular gel films for the first time.

The first GIWAXS pattern (wet sample, Fig. 2A) has a prominent broad peak at 2.00 Å^{-1} with a shoulder at 2.86 Å^{-1} that corresponds to water.[24] Its disappearance over time indicates that drying occurs on all samples. The last pattern (dry sample, Fig. 2B) shows distinct, sharp peaks at low Q at 0.19 Å^{-1} (33.1 Å), 0.17 Å^{-1} (36.9 Å), 0.15 Å^{-1} (41.8 Å) and 0.14 Å^{-1} (44.8 Å) that relate to the unit fibre diameter (the first ordered structural unit formed by the gelator, Table S2, ESI†). Comparison between the first (wet sample) and the last (dry sample) pattern shows the same scattering peaks (a minor shift of 2 Å was only observed for the C10-dCyt gelator) and indicates that the samples are unaffected by the drying process (Fig. 2C). The maintenance of the peak position and enhanced scattering contrast in air favours the subsequent use of dry gel patterns.

For calculation of the fibre diameter, based on previous work for similar nucleolipid systems that form fibrous (cylindrical) structures[15,25] a hexagonal packing is assumed (Fig. S5, ESI†). The calculated C8-dCyt fibre diameter of 38 Å is in close

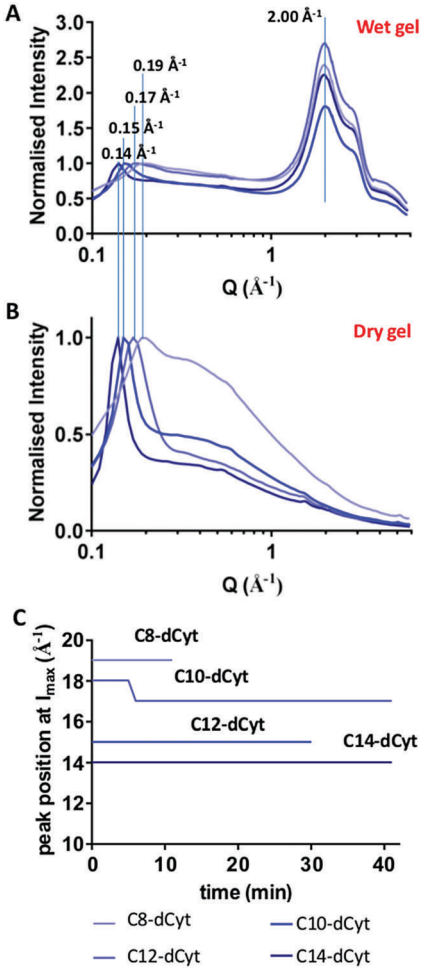

Fig. 2 GIWAXS data of the (A) first (wet sample) and (B) last (dry sample) pattern for all four gelators. Values are normalized to the maximum peak intensity at Q = 0.14 Å^{-1}, 0.15 Å^{-1}, 0.18 Å^{-1} and 0.19 Å^{-1}, for C14-dCyt, C12-dCyt, C10-dCyt and C8-dCyt, respectively. (C) Peak position at maximum intensity as determined from the GIWAXS data is plotted over time for the four gelators. The peak at 2 Å corresponds to water.

agreement with molecular dynamics simulations (36 Å) reported previously.[17] Increasing the alkyl chain length of the gelator causes the calculated fibre diameter to increase linearly from 42.6 Å to 48.3 Å and 51.7 Å for C10-dCyt, C12-dCyt and C14d-Cyt, respectively (Fig. S6, ESI†). This confirms that the alkyl chain length directly impacts the diameter of the self-assembled fibres.

To investigate the arrangement of molecules inside the fibres, the positions of the peak maxima from the GIWAXS data of the dry gels (Fig. 2B) were identified (Table S3, ESI†). All samples showed peak maxima at similar positions that can be assigned structurally in the same manner (Table S3, ESI†), suggesting that the alkyl chain length does not affect the molecular arrangement within the fibres.

The ability of single fibres to associate with each other and form higher order structures such as helices, ribbons, twists and bundles is well documented.[14,15,24,25] In order to explore association of fibres formed by the four different nucleoside based gelators, we used GISAXS. The first collected pattern

(wet gel) was fitted to a flexible cylinder model as previously reported for the C8-dCyt bulk gel.[17] Details of the analysis can be found in ESI,† Section S5. Radii of 59.6 ± 0.7 Å, 53.8 ± 1.6 Å, 50.2 ± 0.3 Å and 61.5 ± 0.3 Å were obtained for the C8-dCyt, C10-dCyt, C12-dCyt and C14-dCyt gels, respectively. The corresponding fibre diameters are significantly larger than the fibre unit diameter reported above, suggesting the formation of higher order structures (fibre bundles).

After establishing that the self-assembled structure of the alkyl modified cytidine gelator can be modulated by changing the alkyl chain length we tested the hypothesis that the chemical composition of the surface could exert a similar effect on the self-assembled architectures. Surfaces were prepared to match specific chemical entities present in the nucleoside gelators; (i) the hydrophobic alkyl chain, (ii) different parts of the nucleoside and (iii) the presence or absence of aromaticity (Fig. S10, ESI†).

Surfaces were functionalized with alkyl chains containing 8 or 18 carbons (C8 and C18), ethylamine ($EtNH_2$), deoxycytidine (dCyt), cytidine (Cyt) cyclohexyl (cHex) and benzyl (Benz) groups. Surface modification was confirmed by water contact angle (WCA) measurements (Table S1, ESI†), ToF-SIMS (Fig. S11 and S12, ESI†) and AFM (Fig. S2, ESI†). All surfaces showed no significant topography and very low surface roughness (R_q < 1.2 nm), making them suitable for GI measurements.

Two of the four gelators, the most hydrophobic (C14-dCyt) and the most hydrophilic (C8-dCyt), were selected to investigate their interaction with the different surfaces. Both gelators self-assemble into fibrous structures (Fig. S13 and S14, ESI†) and form gels on all surfaces.

GIWAXS data were collected on dry gel films formed on all surfaces (Fig. 3). Only dry films were analysed because the water peak obscures the GIWAXS patterns of wet gels and the peak positions on dry and wet films are comparable. The same peaks present in the GIWAXS patterns of C8-dCyt and C14-dCyt on the OH surface were found on all other surfaces, suggesting that neither the unit fibre nor the orientation of the molecules inside the fibres are affected by these surfaces.

To investigate the effect of different surfaces on the higher order structures we collected GISAXS patterns. Peak positions at Q = 0.14 $Å^{-1}$ (C14-dCyt) and 0.19 $Å^{-1}$ (C8-dCyt) remained constant during drying, *i.e.* drying does not change the unit fibre diameter. In contrast, the surface modifications resulted in different fibre bundle radii (Fig. S15, ESI†) that cannot be explained by drying effects (Section S10, ESI†). These fibre bundles were presumably formed by association of individual fibres. This suggests that the effect of the surface is not related to a direct interference in the self-assembly of the gelator molecules. Instead, the surface influences fibre–fibre aggregation which subsequently leads to the formation of thicker fibre bundles.

To exploit surface-mediated self-assembly in the rational design of fibre and gel properties, it is necessary to build a more detailed conceptual understanding of the underpinning surface–gelator interactions from which design rules can emerge. To identify key surface parameters that underpin the observed

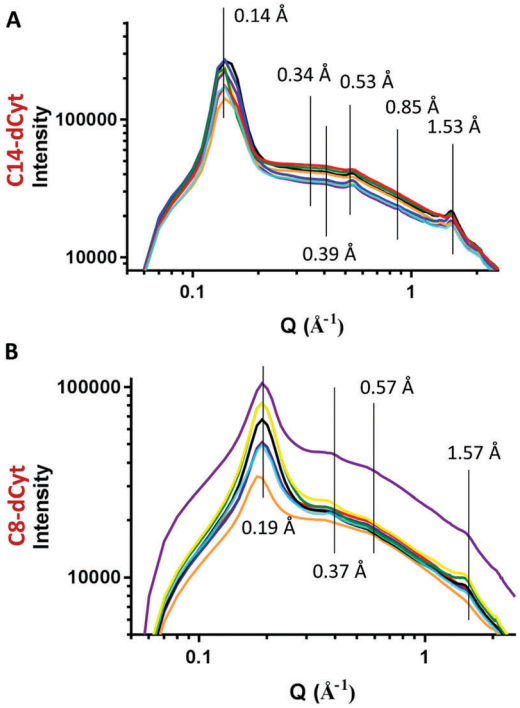

Fig. 3 GIWAXS traces of the dry gels for the two gelators C14-dCyt (A) and C8-dCyt (B) on all the surfaces; cHex (light blue), OH (red), C8 (green), dCyt (blue), Cyt (orange), Benz (purple), C18 (yellow), $EtNH_2$ (black). Peaks are labelled with Q values in $Å^{-1}$.

effect on fibre bundle aggregation, we expressed the chemistry presented on our surfaces with a range of descriptors and tested for correlation of these parameters with the measured fibre bundle radii.

Structural descriptors (number of rotatable bonds), experimental (WCA, R_q) and theoretical (log P, polar surface area (PSA)) parameters (Table S6, ESI†) were used for linear regressions analysis (Table S8, ESI†). PSA and log P correlate linearly with the fibre radii (Fig. 4). Gels deriving from C14-dCyt showed better correlations with the surface properties compared to gels derived from C8-dCyt. Longer aliphatic chains have previously been reported to lead to more effective packing of molecules.[14,26] This in turn improves the quality of scattering patterns and likely contributes to a more accurate fibre radii determination and higher confidence in the correlations for C14-dCyt compared to C8-dCyt.

Higher fibre bundle radii are obtained as PSA increases and log P decreases, *i.e.* fibre bundle radii are related to the hydrophobicity of the immobilised molecules. This is contrasted by the lack of correlation between fibre bundle radii and WCA values, which are descriptors of surface hydrophobicity. Unlike PSA and log P that relate to molecular properties, the WCA is a reflection of surface hydrophobicity, which also depends on surface coverage, orientation of immobilised molecules and surface roughness, among other factors. It is therefore likely that the final self-assembled structures are more sensitive to the nature of the immobilised molecule than the composition of the surface as a whole. The relationship between fibre

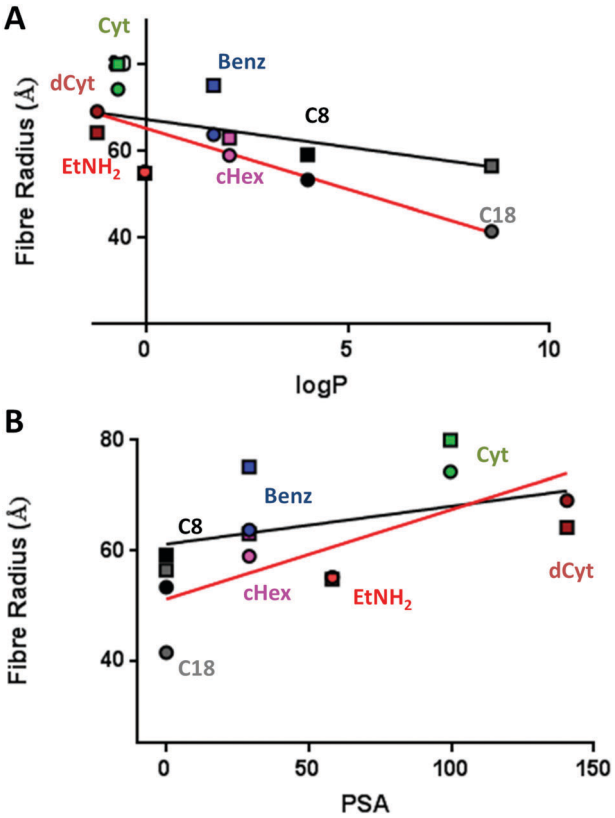

Fig. 4 Linear regression analysis between fibre radius of both gelators and (A) log *P*, R^2 = 0.7678 (C14-dCyt, represented by circles and red trace) and R^2 = 0.2087 (C8-dCyt, represented by squares and black trace) and PSA R^2 = 0.6181 (C14-dCyt, represented by circles and red trace) and R^2 = 0.1448 (C8-dCyt, represented by squares and black trace). The datapoints are labelled to indicate the respective surface chemistry: alkyl chains containing 8 or 18 carbons (C8 and C18), ethylamine ($EtNH_2$), deoxycytidine (dCyt), cytidine (Cyt), cyclohexyl (cHex) and benzyl (Benz) groups (Fig. S10, ESI†).

bundle radii and aromaticity was tested with a *t*-test ($P < 0.05$). The presence of an aromatic ring leads to higher fibre bundle diameters, also supporting the concept that specific chemistries affect fibre bundle formation.

Conclusions

In summary, we used GIWAXS and GISAXS to investigate the interfacial interactions between a class of gelators with different hydrophobicities and surfaces with a range of different chemistries for the first time and determine how these parameters affect the final supramolecular structures formed on the surfaces. We demonstrated that the size of the hydrophobic alkyl chain in the gelator directly affects gel fibre diameter. In contrast, the chemical nature of the surface did not influence the fibre diameter but affected the aggregation of fibres. This leads to formation of fibre bundles with radii whose size correlates with the hydrophobicity of the surface immobilised molecules (log *P*, polar surface area, aromaticity). The fact that the fibre radii do not correlate with experimental descriptors of the overall surface (WCA, R_q) indicates that the chemical nature of the immobilised molecules is more important than the overall surface properties. We believe that identifying the nature of the surface–gelator interactions and the parameters that control them will enable significantly improved design of self-assembly processes and their tailoring to emerging applications in material and life sciences.

Experimental methods

Gel film preparation

The gelators were weighed out in 1.5 ml scintillation vials and ethanol was added to achieve a stock concentration of 25 mg ml^{-1}. The vial was transferred on a preheated hotplate at 60 °C and heated up for 2 minutes (complete dissolution). Water was added to achieve a final concentration of 5 mg ml^{-1} and the sample was immediately transferred onto a silicon wafer for further analysis.

Grazing incidence X-ray diffraction (GID) and grazing incidence small angle X-ray scattering (GISAXS)

GIWAXS and GISAXS experiments were performed on the I07 beamline, Diamond Light Source,[27] Didcot, UK using a Pilatus P2M detector. Surfaces were aligned and time-resolved GIWAXS experiments were started immediately after spreading of the solution on the surface using X-rays with an energy of 18 keV and a wavelength of 0.68728 Å to achieve a *Q*-range of 0.05 $Å^{-1}$ to 5.8 $Å^{-1}$. The sample-detector distance was 30 cm. For time resolved GISAXS experiment, patterns with a *Q*-range of 0.027–0.6 $Å^{-1}$ were obtained using an X-ray energy of 14.5 keV and a wavelength of 0.855 Å. The sample-detector distance was 3 m. In both cases the incident angle was 0.08°, just below the critical angle for the substrate and ensuring surface sensitivity. For GIWAXS, 20 μl of warm gelator solution were spread on each surface whereas 10 μl were used for GISAXS. The different sample volumes in the GISAXS experiment were in order to achieve shorter drying times for all the time-resolved data to be collected. Samples were initially aligned before spreading the solution and time-resolved data were recorded directly after the solution was spread. A pattern was collected every two minutes. The first pattern collected from GISAXS data was fitted using SasView-4.1 as explained in the ESI.† Statistical analysis was performed with GraphPad Prism 7 and the outcome is tabulated on ESI,† Table S8.

Details of the experimental methods describing the surface modifications, surface characterisation, AFM imaging of the gels and statistical analysis are included in the ESI.†

Conflicts of interest

There are no conflicts to declare.

Acknowledgements

This work was support by the Engineering and Physical Sciences Research Council [grant number EP/L01646X] *via* the

CDT in Targeted Therapeutics grant and the Leverhulme Trust [grant number RPG-2016-199] *via* a research project grant and the Diamond Light source [experiment number SI16246] *via* beamtime access for GIWAXS and GISAXS measurements.

References

1 N. M. Sangeetha and U. Maitra, *Chem. Soc. Rev.*, 2005, **34**, 821–836.
2 J. W. Steed, *Chem. Commun.*, 2011, **47**, 1379–1383.
3 M. C. Branco and J. P. Schneider, *Acta Biomater.*, 2009, **5**, 817–831.
4 K. J. Skilling, F. Citossi, T. D. Bradshaw, M. Ashford, B. Kellam and M. Marlow, *Soft Matter*, 2014, **10**, 237–256.
5 P. Schaaf, C. Vigier-Carrière, F. Boulmedais and L. Jierry, *Angew. Chem.*, 2017, **57**, 1448–1456.
6 B. Yang, D. J. Adams, M. Marlow and M. Zelzer, *Langmuir*, 2018, DOI: 10.1021/acs.langmuir.1028b01165.
7 P. Kumaraswamy, R. Lakshmanan, S. Sethuraman and U. M. Krishnan, *Soft Matter*, 2011, **7**, 2744–2754.
8 V. V. Korolkov, S. Allen, C. J. Roberts and S. J. Tendler, *Faraday Discuss.*, 2013, **166**, 257–267.
9 E. Mayans, G. Fabregat, R. Juárez, C. Cativiela, J. Puiggalí and C. Alemán, *ChemistrySelect*, 2017, **2**, 1133–1139.
10 R. Huang, R. Su, W. Qi, J. Zhao and Z. He, *Nanotechnology*, 2011, **22**, 245609.
11 M. G. F. Angelerou, A. Sabri, R. Creasey, P. Angelerou, M. Marlow and M. Zelzer, *Chem. Commun.*, 2016, **52**, 4298–4300.
12 S. Han, S. Cao, Y. Wang, J. Wang, D. Xia, H. Xu, X. Zhao and J. R. Lu, *Chem. – Eur. J.*, 2011, **17**, 13095–13102.
13 I. W. Fu, C. B. Markegard, B. K. Chu and H. D. Nguyen, *Langmuir*, 2014, **30**, 7745–7754.
14 A. Nuthanakanti and S. G. Srivatsan, *Nanoscale*, 2016, **8**, 3607–3619.
15 V. Allain, C. Bourgaux and P. Couvreur, *Nucleic Acids Res.*, 2011, **40**, 1891–1903.
16 J. Raeburn, A. Z. Cardoso and D. J. Adams, *Chem. Soc. Rev.*, 2013, **42**, 5143–5156.
17 M. Angelerou, P. W. Frederix, M. Wallace, B. Yang, A. Rodger, D. J. Adams, M. Marlow and M. Zelzer, *Langmuir*, 2018, **34**, 6912–6921.
18 J. Baillet, V. Desvergnes, A. Hamoud, L. Latxague and P. Barthélémy, *Adv. Mater.*, 2018, **30**, 1705078.
19 B. Alies, M. A. Ouelhazi, A. N. Patwa, L. Navailles, V. Desvergnes and P. Barthelemy, *Org. Biomol. Chem.*, 2018, **16**, 4888–4894.
20 C. Montis, Y. Gerelli, G. Fragneto, T. Nylander, P. Baglioni and D. Berti, *Colloids Surf., B*, 2016, **137**, 203–213.
21 K. J. Skilling, B. Kellam, M. Ashford, T. D. Bradshaw and M. Marlow, *Soft Matter*, 2016, **12**, 8950–8957.
22 J. Als-Nielsen, D. Jacquemain, K. Kjaer, F. Leveiller, M. Lahav and L. Leiserowitz, *Phys. Rep.*, 1994, **246**, 251–313.
23 G. Renaud, R. Lazzari and F. Leroy, *Surf. Sci. Rep.*, 2009, **64**, 255–380.
24 A. Aggeli, I. A. Nyrkova, M. Bell, R. Harding, L. Carrick, T. C. McLeish, A. N. Semenov and N. Boden, *Proc. Natl. Acad. Sci. U. S. A.*, 2001, **98**, 11857–11862.
25 G. M. Peters and J. T. Davis, *Chem. Soc. Rev.*, 2016, **45**, 3188–3206.
26 A. Nuthanakanti and S. G. Srivatsan, *ACS Appl. Mater. Interfaces*, 2017, **9**, 22864–22874.
27 C. Nicklin, T. Arnold, J. Rawle and A. Warne, *J. Synchrotron Radiat.*, 2016, **23**, 1245–1253.